Chapter

Analysis of Diesel Particulate Matter Flow Patterns in Different Ventilation and Operational Conditions of Underground Mines

Ramakrishna Morla, Shivakumar Karekal and Ajit Godbole

Abstract

Diesel-operated vehicles are commonly used by personnel in underground mines. Although these vehicles facilitate travel within the mine, their main disadvantage is that they generate diesel particulate matter (DPM), a known carcinogenic agent. This calls for research to control the spread of DPM in underground mines in order to ensure the safety of mine personnel. In this article, the flow patterns of DPM generated by two types of diesel-operated vehicles are modeled using computational fluid dynamics (CFD) simulations. The simulation results are validated using field experimental measurements. The models show that if the vehicle is stationary, DPM particles are dispersed towards the center of the gallery and occupy the entire cross section of the road way. Vehicle movement induces air currents that may result in the miners being exposed to high DPM concentrations. The results show that if the DPM and the intake air counter-flow (flow in opposite directions), the DPM spread occurs throughout the entire cross-section of the roadway. This research is expected to contribute to the formulation of effective DPM control strategies in underground mines.

Keywords: underground mines, DPM, diesel-powered man riding vehicle

1. Introduction

As underground mines go ever deeper and spread over larger areas in an attempt to meet ever-increasing production targets, there is a correspondingly significant increase in the usage of diesel-powered vehicles. Most of the mines in the world have been using diesel-operated vehicles for transportation of men, material, ore, waste rock, coal and for various other mining operations. The commonly used diesel-operated vehicles in underground coal, metal and non-metal mines are trucks, load haul dumpers (LHD), Jumbos, cable bolters, long hole drilling rigs, man-riding vehicles, telehandlers, graders, water tankers, forklifts, articulated wheel loaders, agitators, shotcrete sprayers, etc.

Diesel-powered vehicles offer greater flexibility than electric and battery-operated vehicles because they can travel over longer distances and between working sections. The use of diesel vehicles is efficient, as evidenced by ease of

maintenance, consistency and durability. Many nations have depended on these vehicles for these reasons [1].

Diesel is a mixture of hydrocarbons. In a perfect diesel engine, oxygen (O_2) from the air converts all the hydrogen (H_2) in the fuel to H_2O and the carbon (C) to CO_2, while the nitrogen (N_2) in the air remains unaffected. But in the reality, the combustion process is not perfect, and the engine emits several pollutants due to incomplete combustion [2].

$$\text{Fuel} + \text{Air} \rightarrow \text{Unburned hydrocarbons} + NO_x + CO_2 + CO + \text{Water} \quad (1)$$

The diesel engine exhaust fumes mainly contain a mixture of diesel particulate matter (DPM) and other pollutant gases such as nitrogen oxides (NO_x), hydrocarbons (HC), including either total hydrocarbons (THC) or non-methane hydrocarbons (NMHC) and carbon monoxide (CO) [3].

Different nations recommend different safe occupational exposure limits (OEL). **Table 1** shows the OEL used in Australian underground mines.

The ventilation air requirement to dilute any of the gases (CO, CO_2, SO_2, NO and NO_2) or DPM emitted by a diesel engine to the targeted concentration level (Q_v) can theoretically be calculated for any given movement using the following equation [2]:

$$Q_V\left[m^3/s\right] = \frac{Q_E[m^3/s]\ X\ (C_E\ [ppm\ or\ \mu g/m^3] - C_T\ [ppm\ or\ \mu g/m^3])}{C_T\ [ppm\ or\ \mu g/m^3] - C_B\ [ppm\ or\ \mu g/m^3]} \quad (2)$$

Where Q_E is exhaust flow rate, C_E is the concentration of the specific pollutant (gas or DPM) in the exhaust, C_T is target concentration of the corresponding gas or DPM and C_B is the concentration of the specific pollutant (gas or DPM) in the dilution air.

As per the Australian Mines Regulations and Act [4–6], to minimize exposure of mine personnel to diesel emissions, the mine operator must collect diesel engine

Contaminant	OEL (TWA 8)	OEL (TWA 10)	OEL (TWA 12)	OEL (STEL)*
Carbon dioxide—CO_2 (ppm)**	5000	3500	2500	30,000
Carbon monoxide—CO (ppm)**	30	21	15	—
Nitrogen dioxide—NO_2 (ppm)**	3	2.1	1.5	5
Nitrous oxide—NO (ppm)**	25	17.5	12.5	—
Sulfur dioxide (ppm)	2	1.4	1	5
Diesel particulate matter—total particulate—DPM (mg/m^3)***	0.16	—	—	—
Elemental carbon—EC (mg/m^3)***	0.1	—	—	—

Where, TWA 8 is 8-hour time weighted average and STEL is short term exposure limit.
**STEL refers to the maximum concentration where personnel can work for a maximum of 15 minutes at a time. A maximum of 1 hour per shift can be allowed provided that it is broken up into four 15-minute work intervals, with a minimum 1-hour break in between work intervals.*
***Gases are treated as acute hazards; therefore, reduction factors based on hours worked per shift can be applied to the standard OEL (TWA 8). A 10-hour shift will have a reduction factor of 0.7 and 12-hour shift will have a reduction factor of 0.5 applied to the target gas.*
****Particles are treated as chronic hazards. The OEL (TWA 8) needs to be adjusted according to the shift roster worked by the work group. Reference can be made to the formula: Reduction factor = 170/x where x is the number of hours worked per month.*

Table 1.
Workplace exposure limits of diesel vehicle emissions [3].

exhaust samples in underground mines and analyze the samples. The results of the analysis are compared with the baseline exhaust emissions for the diesel engine. All underground diesel engines are regularly maintained so that emissions from the engine are as low as is reasonably practicable with respect to the base line exhaust emissions. The mine operator must also maintain the standard fuel or fuel additive quality and DPM filters.

1.1 DPM

The chemical composition of DPM depends on the compositions of the fuel and the lubricating oil, engine technology, operating conditions, and the technology used to treat the exhaust. The major contributors to the total particle mass emitted by diesel engines include elemental carbon (EC), organic carbon (OC), inorganic ions such as sulfates, nitrates, ammonia, sodium, chloride ions, and trace metallic compounds [2].

EC and OC emissions, cumulatively known as 'total carbon (TC)', make up the largest fraction of aerosols emitted by diesel engines. TC is generally considered to make up about 70–90% of DPM. On an average, elemental carbon comprises 50–70% of TC and greater than 45% of 'total engine-out' DPM emissions. The engine-out organic carbon makes up between 10 and 80% of total carbon [2].

The EC fraction of DPM is a product of the pyrolysis of the fuel and the lubricating oil in the combustion chamber. The OC fraction of exhaust emissions from a diesel engine is a complex mixture of burned and unburned lubricating oil and fuel compounds.

1.2 DPM size distribution

DPM particles are very small and are subdivided into three categories with respect to size: Nano-particles less than 50 nm in diameter, ultra-fine particles less than 100 nm in diameter and fine particles less than 2.5 μm in diameter. **Figure 1** shows a typical DPM size distribution weighted by number, surface area, and mass [7].

The DPM is composed of numerous small particles with very little mass, mixed with relatively few larger particles, which contain most of the total mass. A small fraction of diesel particles resides in the third, 'coarse' mode.

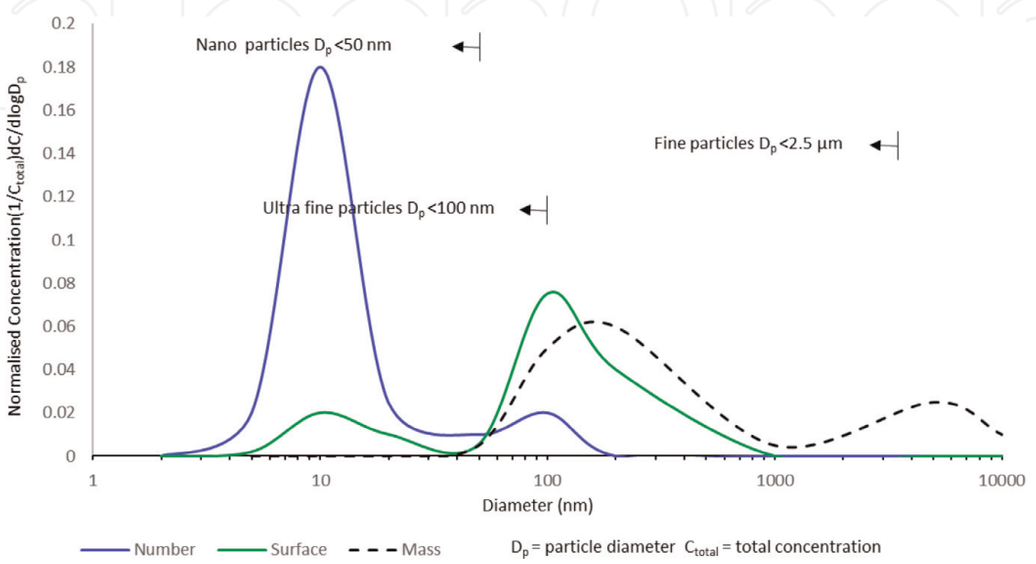

Figure 1.
DPM particles size distribution [7].

The DPM particles of size ranging from 3 to 500 nm are more dangerous for human health. These particles can get lodged in the alveolar regions of the longs where gas exchange takes place [2].

Various research studies have been conducted to better understand the effects of DPM on human health [1, 8–10]. These studies have concluded that exposure to diesel exhaust may cause cancer in humans.

The effective density of DPM decreases sharply from 1.2 g/cm^3 for 30 nm particles to 0.3 g/cm^3 for 300 nm particles. The effective density of agglomerated diesel particles varies from 1.1 to 1.2 g/cm^3. The chemical composition of DPM has not been observed to follow any trend and it mainly depends on engine oil and diesel chemical composition [11].

1.3 Workplace exposure limits on DPM in underground mines

Different countries follow different workplace exposure limits and mine ventilation standards to deal with DPM. **Table 2** shows a summary of DPM exposure limits and ventilation requirements. The regulations in different countries are outlined in the following sections.

Country		DPM exposure limits (μg/m^3)	Ventilation standards
	British Columbia	1500 (RCD)	Ventilation as per CSA, minimum 0.06 m^3/kWs
Canada	Alberta	ACGIH	Minimum air volume of 1.9 m^3/s at active headings, and minimum air velocity 0.3 m/s
	Saskatchewan	—	Ventilation as per CANMET approval, minimum of 0.06 m^3/kWs
	Manitoba	ACGIH	Ventilation as per CANMET or MSHA approval, or 0.092 m^3/kWs for non-approved engine
	Ontario	400 (RCD)	Minimum ventilation of 0.06 m^3/kWs
	Quebec	600 (RCD)	Ventilation as per CANMET or MSHA approval, or 0.092 m^3/kWs for non-approved engine
	New Brunswick	1500 (RCD)	Minimum ventilation of 0.067 m^3/kWs
	Nova Scotia	1500 (RCD)	Minimum air velocity 0.33 m/s
	Newfoundland & Labrador	ACGIH	Engine approval is required from the Chief Inspector of mines minimum ventilation of 0.047 m^3/kWs
	Northwest, Yukon & Nunavut	1500 (RCD)	Minimum ventilation of 0.06 m^3/kWs
China		—	Minimum ventilation of 0.067 m^3/kWs
South Africa		N/A	Minimum ventilation of 0.063 m^3/kWs
USA		160 (TC)	As per MSHA certificate
India		100 (EC)	Minimum ventilation of 0.06 m^3/kWs
Germany		100 (EC)	Minimum ventilation of 0.06 m^3/kWs

MSHA: Mine Safety and Health Administration.
ACGIH: American Conference of Governmental Industrial Hygienists.
RCD: Respirable Combustible Dust.
CANMET: Canada Centre for Mineral and Energy Technology.

Table 2.
International DPM exposer limits and ventilation standards [12].

As per the Australian Coal Mines Work Health and Safety (WHS) Regulations 2006 [6], WHS (mines) Act 2013 [5] and WHS (mines) Regulations 2014 [4], the maximum allowable workplace exposure (mine atmosphere) for DPM in the elemental carbon (EC) form when expelled from a diesel engine is 0.1 mg/m^3. This is approximately equal to 0.16 mg/m^3 of TC or 0.2 mg/m^3 DP.

As per Australian WHS mines act and regulations, the volume of air in each place where a diesel engine operates must be such that a ventilating current of not less than:

- 0.06 m^3/s for each kilowatt of maximum output capacity of the engine, or
- 3.5 m^3/s,

The ventilation air flow is directed along the airway in which the engine operates. If more than one diesel engine is being operated in the same ventilating current, the engine kilowatts must be added, and the minimum ventilation requirement is 0.06 m^3/s/kW or 3.5 m^3/s, whichever is greater.

The minimum mine ventilation quantity to dilute diesel particulate exhaust emissions to 0.1 mg/m^3 (diesel particulate signature) $Q_{DP(min)}$ can be calculated using the following equation [3]:

$$Q_{DP(min)} = \frac{EC_{kW}}{3600DP_{(Exposure\ limit)}} P_{WA} \tag{3}$$

where $Q_{DP(min)}$ is minimum mine ventilation quantity (m^3/s), $DP_{(Exposure\ limit)}$ is 0.1 EC (mg/m^3), EC_{kW} = sum of weighted average diesel particulate (EC) per hour emitted from the diesel engine exhaust over the specified duty cycle (mg/h) and PWA is sum of weighted average power for the diesel engine over the duty cycle (kW).

1.4 Previous DPM field investigations in underground mines

The National Institute of Occupational Health and Safety (NIOSH) organized a detailed DPM field study on the effectiveness of diesel-vehicle filters and bio-diesel in isolated underground environment at the Nye Mine run by the Stillwater Mining Company [13]. This study was conducted by a partnership formed by NIOSH, the National Mining Association (NMA), the National Stone, Sand and Gravel Association (NSSGA), the United Steel Workers of America (USWA) and the MARG Diesel Coalition [13]. Two trucks and three load haul dumpers (LHDs) were used for this experiment. The main aim of this study was to study the effectiveness of the diesel particulate filter (DPF) systems. In this study, the tested DPF systems were Engelhard DPX, DCL MineX, Clean Air System, DCL Blue Sky, Mac's Mining Repair/Donaldson P604516, ECS Cattrap and Biodiesel [13].

Subsequently, the effectiveness of the DPF systems to control DPM and gases was assessed under the diesel emissions evolution program (DEEP). This study was conducted at an isolated mine zone of Narannda's Brunswick Mine in Bathurst. This study involved the Burnswick mine, Natural Resources Canada, Canada Centre for Mineral and Energy Technology (CANMET), National Institute of Occupational Safety and Health (NIOSH), Andreas Mayer of VERT and DPF systems suppliers [14]. Four 242 kW LHDs and two 278 kW haulage trucks were used for this study. The tested DPF systems were ECS catalyzed filter, ECS octel filter, DCL catalyzed/electric filter and Oberland Mangold octel filter [14].

Recently, as a part of Ph.D. research, a DPM field study has been conducted at an experimental mine at the Missouri University of Science and Technology. The aim of the research was to study DPM dispersion in underground metal/non-metal mines [15]. A 30 kW Skid-steer loader was used for this study [15].

A greater understanding of DPM flow patterns in different conditions will help control the miners' exposure to the high concentrations of DPM in the vicinity of diesel-operated vehicles. This chapter describes a detailed study of DPM flow patterns generated by diesel-operated man-riding vehicles and LHDs, using field experiments and computational fluid dynamics (CFD) investigations. The field experiments and CFD simulation studies were conducted in two stages: stage 1 with a man-riding vehicle and stage 2 with an LHD, both with different air flow directions.

2. Experimental investigation

2.1 The experimental site

Field experiments were conducted in an Indian coal mine, 'mine A', in one of the eight working seams in the mine. The mine has a number of bord and pillar and long wall working sections. The mine uses diesel-operated man-riding vehicles, LHDs and shuttle cars. The ventilation system of the mine consists of five intakes and two return shafts with two main axial flow fans. The operating parameters of the two fans are: air flow of 150 m^3/s at 510 Pa pressure and air flow of 140 m^3/s at 400 Pa pressure respectively.

2.2 Details of field experiment 1

A calibrated 'Airtec' real-time DPM monitoring instrument was used for these field experiments. This instrument measures the concentration of elemental carbon (EC) or total carbon (TC) in real time. This instrument works on the principle of laser diode absorption technique [16, 17]. This monitor uses technology developed by the diesel particulate group at the NIOSH Pittsburgh Research Laboratory and has been determined to precisely replicate results from their method 5040 test. This monitor can help prevent safety non-compliances, ensuring increased miner safety [18].

The flow rate and sampling time of the DPM monitor was adjusted to 2.83×10^{-5} m^3/s (1.7 liters per minute) and 5 minutes respectively. Before the experiment, the location of vehicle, smoke pipe (DPM source), sampling stations were determined and marked on the gallery. During the experiment, the vehicle position was not changed. An average of three 5-minute sample were taken at each sampling station.

Figure 2 shows the locations and arrangements of sampling stations and sampling points (a, b and c). During this experiment, the engine was run under a 'no-load' condition.

To ensure that the intake air was devoid DPM, the experiment was conducted in one of the intake airways near the bottom of the shaft. The length, width and height of the gallery were measured to be 100, 6 and 2.7 m respectively. During the experiment, the intake air velocity was maintained at 1.26 m/s. The velocity and temperature of the vehicle exhaust fumes were measured to be 29 m/s and 323 K respectively.

2.3 Details of field experiment 2

In this experiment, the LHD exhaust smoke was directed opposite to the ventilation air flow. DPM samples were measured downstream side of the LHD. In this case, DPM samples were collected around the LHD and also at 6, 10 and 20 m downstream of the LHD at a height of 1.2 m from the floor. At each sample station, three samples were measured, each over a 5-minute duration. The average of the three readings was considered as representative of that sample station.

Figure 3 shows the location and details of the sampling points. DPM was measured at 11 sampling stations, **Figure 3**. During this experiment, the air flow in the experimental gallery was 20.4 m^3/s.

As in field experiment 1, the flow rate and sampling time of the DPM monitor was adjusted to 2.83×10^{-5} m^3/s (1.7 liters per minute) and 5 minutes respectively. Before the experiment, location of vehicle, smoke pipe, sampling stations were measured and marked on the gallery. During the experiment, the vehicle position was not changed. Average of three 5-minute samples were taken at each sampling station.

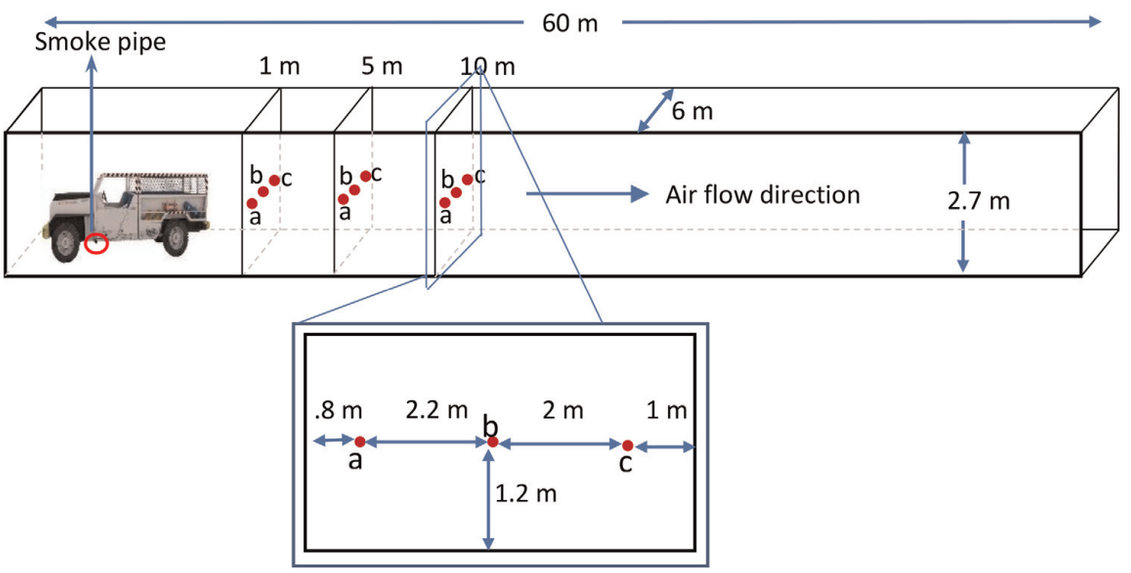

Figure 2.
Locations of sampling stations and sampling points w.r.t DPM source (vehicle).

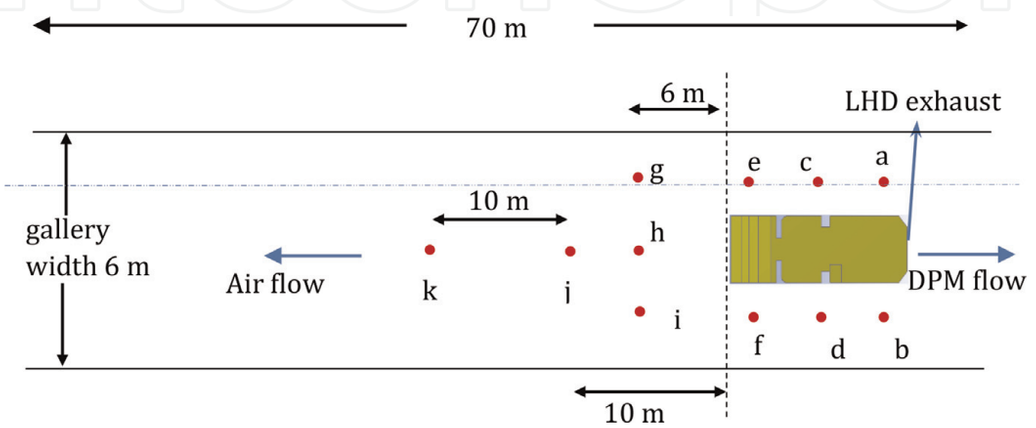

Figure 3.
Locations of sampling stations and sampling points, top view.

3. CFD modeling

CFD modeling techniques have been used to study the flow patterns of DPM generated by 30 kW stir skid loaders in metal mines [15, 19–22]. More recently, CFD simulations of the dispersion of DPM generated by diesel-driven man-riding vehicles in coal mines have been reported [23, 24]. Here, we present simulations of DPM generated by a diesel-operated man-riding vehicle and an LHD/loader/utility vehicle in an underground coal mine. The commercially available CFD package ANSYS Fluent (v. 19.1) was used.

3.1 Construction of computational domain and mesh for experiment-1

A 60-m long ventilation gallery was designed for simulations width and height of the gallery were 6 and 2.7 m. Man riding vehicle was designed and imported from the 3D CAD modeling. The overall dimensions of the man-riding were length 6.25 m, width 2 m and height 1.95 m. The location of the smoke pipe (DPM source) was just behind the left front wheel on the opposite side to the vehicle operator. The engine was equipped with a diesel particulate filter and the exhaust flow was a mixture of DPM and air. **Figure 4** shows the details of the constructed CFD model.

Figure 5 shows the details of the surface mesh on the man riding vehicle (a) and man riding vehicle with gallery (b). To achieve accurate results, finer mesh was used with half-million computational cells. The minimum size of the cells was 7.3×10^{-3} m, minimum edge length of cells was 0.025 m and size function was 'proximity and curvature'. The program-controlled 'inflation' feature was used with seven layers was used to generate finer cells in the boundary layers adjacent to solid boundaries.

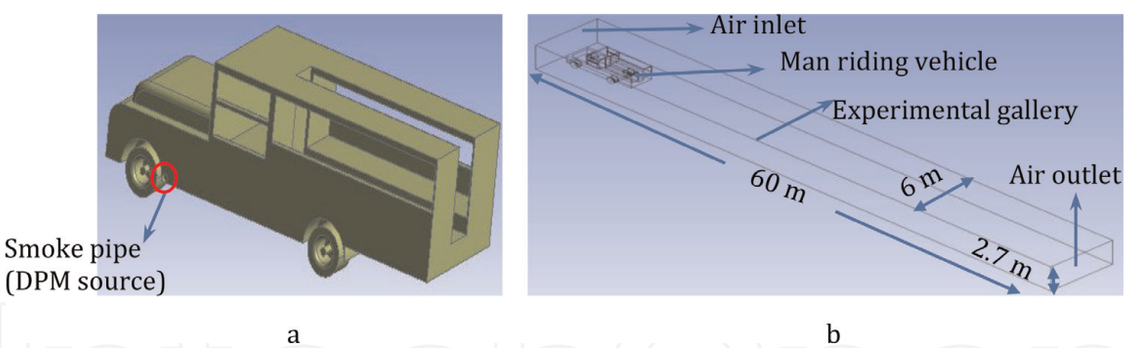

Figure 4.
CFD model of man riding vehicle and experimental gallery. (a) Man riding vehicle—CAD model. (b) Experimental gallery.

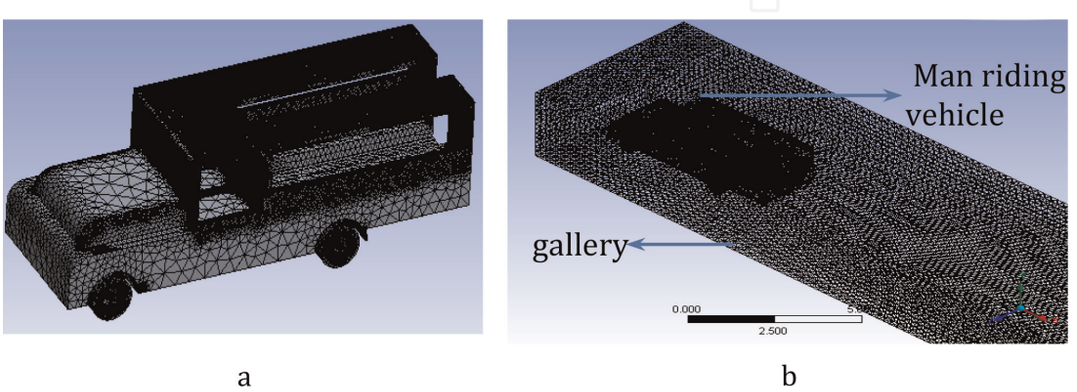

Figure 5.
Mesh model of man riding vehicle and experimental gallery. (a) Surface mesh on man riding vehicle. (b) Mesh for airway.

3.2 Construction of computational domain and mesh for experiment-2

The computational domain is a 70 m long tunnel with a rectangular cross section (width 6 m, height 2.7 m). A CAD model of an LHD vehicle was designed and imported into the computational domain. The location of the exhaust is at the rear end of the LHD. The exhaust flow is a mixture of DPM and air. **Figure 6(a)** shows the CAD model representing the vehicle, and **Figure 6(b)** shows the experimental gallery with LHD. **Figure 7(a)** shows the mesh generated for the complex surfaces of the vehicle and (b) shows the details of the computational domain and mesh made up of about half-million computational cells. Finer cells were used to capture details of the flow in regions such as small gaps and adjacent to solid surfaces.

3.3 Setting up the flow conditions

Intake air was supplied through the inlet of the gallery with 1.26 m/s velocity for experiment-1 and 2 m/s for experiment-2 at 300 K temperature. DPM was released from the smoke pipe with a velocity of 29 m/s and temperature of 323 K. For these investigations, DPM is treated as a gas, chemical reactions were not considered. The Boussinesq approximation was used to simulate buoyancy and the effect of turbulence was taken into account.

3.4 Governing equations

To model turbulent flow of mine air, Reynolds-Averaged Navier-Stokes equation was used. In Reynold's averaging, the solution variables in the exact

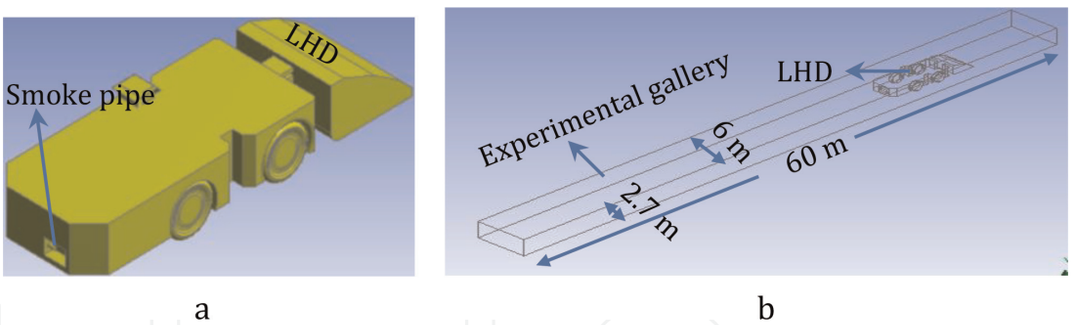

Figure 6.
CFD model of man riding vehicle and experimental gallery. (a) LHD—CAD model. (b) Experimental gallery with LHD.

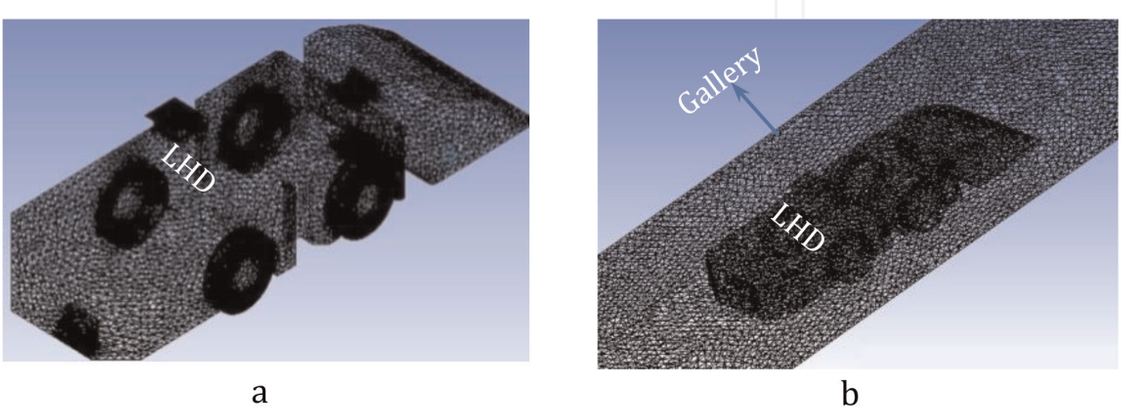

Figure 7.
Surface mesh on LHD & mesh in gallery with LHD. (a) Surface mesh of LHD. (b) Surface mesh of LHD & gallery.

Navier-Stokes equations are consisting of time averaged and fluctuated components for velocity components [25].

$$u_i = \overline{u}_i + u_i' \tag{4}$$

Where $\bar{u}_i$ and u_i' are mean and fluctuating velocity components (i = 1, 2, 3).

Reynolds-averaged Navier-Stokes (RANS) equation was obtained by substituting time and average velocity in momentum equation:

$$\frac{\partial \rho}{\partial t} + \frac{\partial}{\partial x_i}(\rho u_i) = 0 \tag{5}$$

$$\frac{\partial}{\partial x}(\rho u_i) + \frac{\partial}{\partial x_j}\left(\rho u_i u_j\right) = -\frac{\partial p}{\partial x_i} + \frac{\partial}{\partial x_j}\left[\mu\left(\frac{\partial u_i}{\partial x_j} + \frac{\partial u_j}{\partial x_i} - \frac{2}{3}\delta_{ij}\frac{\partial u_l}{\partial x_l}\right)\right] + \frac{\partial}{\partial x_j}\left(-\rho\,\overline{u_{i'}\,u_{j'}}\right) \tag{6}$$

Where $-\rho\,\overline{u_{i'}\,u_{j'}}$ is Reynolds stress can be solved with Boussinesq hypothesis and Reynolds stress models (RSM). In Boussinesq hypothesis, the Reynolds stress are related to the mean velocity gradient [25].

$$-\rho\,\overline{u_{i'}\,u_{j'}} = \mu_t\left(\frac{\partial u_i}{\partial x_j} + \frac{\partial u_j}{\partial x_i}\right) - \frac{2}{3}\left(\rho k + \mu_t\frac{\partial u_k}{\partial x_k}\right)\delta_{ij} \tag{7}$$

To determine turbulent viscosity μ_t, $k-\varepsilon$ model was used.

$$\mu_t = \rho C_\mu \frac{k^2}{\varepsilon} \tag{8}$$

Where C_μ is a constant, k is the turbulence kinetic energy and ε is the turbulent dissipation rate and turbulent heat transport is modeled using the concept of the Reynolds analogy to turbulent momentum transfer. The modeled energy equations are as follows:

$$\frac{\partial}{\partial t}(\rho E) + \frac{\partial}{\partial x_i}\left[u_i(\rho E + p)\right] = \frac{\partial}{\partial x_j}\left[\left(k + \frac{c_p\mu_t}{\sigma_k}\right)\frac{\partial T}{\partial x_j} + u_i\left(\tau_{ij}\right)_{eff}\right] + S_h \tag{9}$$

Where k is the thermal conductivity, E is the total energy and $\left(\tau_{ij}\right)_{eff}$ is the deviatoric stress tensor, defined as

$$\left(\tau_{ij}\right)_{eff} = \mu_{eff}\left(\frac{\partial u_j}{\partial x_i} + \frac{\partial u_i}{\partial x_j}\right) - \frac{2}{3}\mu_{eff}\frac{\partial u_k}{\partial x_k}\delta_{ij} \tag{10}$$

The standard k-ε model is based on the model transport equations for the turbulence kinetic energy (k) and its dispersion rate (ε). The model transport equation for k is derived from the exact equation, while the model transport equation for ε was obtained using physical reasoning and bears little resemblance to its mathematically exact counterpart.

In the derivation of the k-ε model, the assumption is that the flow is fully turbulent, and the effect of molecular viscosity is negligible. As the mine air considered as fully turbulent flow, k-ε model is valid for mine air.

The turbulent kinetic energy, k, and its rate of dissipation, ε, are obtained from the following governing equations [25]:

$$\frac{\partial}{\partial t}(\rho k) + \frac{\partial}{\partial x_i}(\rho k u_i) = \frac{\partial}{\partial x_j}\left[\left(\mu + \frac{\mu_t}{\sigma_k}\right)\frac{\partial k}{\partial x_j}\right] + G_k + G_b - \rho\varepsilon - Y_M + S_k \tag{11}$$

$$\frac{\partial}{\partial t}(\rho\varepsilon) + \frac{\partial}{\partial x_i}(\rho\varepsilon u_i) = \frac{\partial}{\partial x_j}\left[\left(\mu + \frac{\mu_t}{\sigma_\varepsilon}\right)\frac{\partial \varepsilon}{\partial x_j}\right] + C_{1\varepsilon}\frac{\varepsilon}{K}(G_k + C_{3\varepsilon}G_b) - C_{2\varepsilon}\rho\frac{\varepsilon^2}{K} + S_\varepsilon \tag{12}$$

Where G_b is the generation of turbulence kinetic energy due to buoyancy, G_k is the production of turbulence kinetic energy due to the mean velocity gradient, Y_M is the contribution of the fluctuating dilation in compressible turbulence to the overall dissipation rate, $C_{1\varepsilon}$, $C_{2\varepsilon}$ and $C_{3\varepsilon}$ are constants. S_k and S_ε are user defined source terms.

4. Results and discussions

4.1 Experiment 1

Figure 8 shows the DPM cloud in top view. From the figure, high DPM concentration is seen between the smoke pipe side of the vehicle and wall. No DPM concentration is observed near the operator and passenger seat. Downstream of the vehicle, DPM particles spread throughout the whole gallery.

Figure 9 shows the DPM concentration at 1 and 5 m downstream to the vehicle. At 1 m downstream to the vehicle, **Figure 9(a)** shows that the maximum DPM concentration is near the left half of the roof and the side. Traces of DPM are observed in the blue-green band across the airway, and negligible concentration on the right side. **Figure 9(b)** shows the DPM concentration at 5 m downstream to the vehicle. The DPM is seen to flow towards the smoke pipe side of the roadway. The maximum DPM concentration is near the middle of the roadway. **Figure 9(c)** shows the DPM concentration at 10 m downstream to the vehicle. DPM concentration at the middle of the road way is 110 μg/m^3 and the right side of the road way 57 μg/m^3.

4.2 Experiment-1 model validation

Table 3 compares the field measurements with results of the CFD simulations. The CFD results are seen to be in fair in agreement the field data, with the difference varying from −14.2 to +14%. In some cases, the simulated values are different

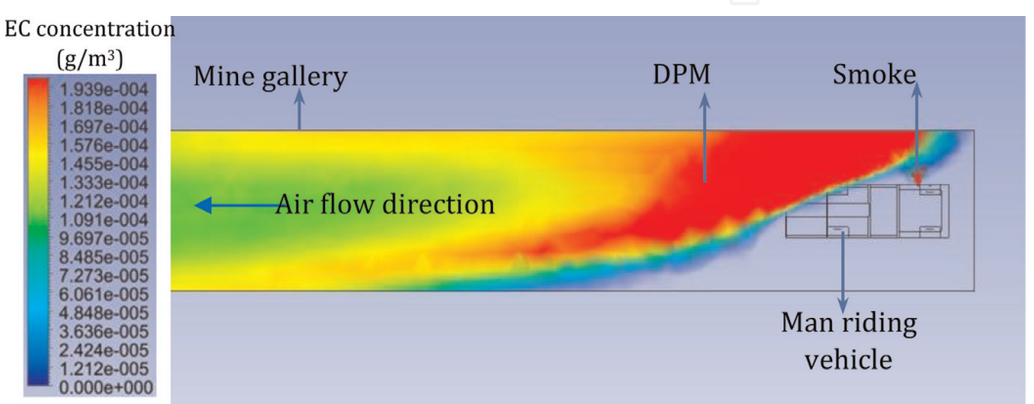

Figure 8.
DPM flow pattern—top view, 2D concentration contours in a plane near the ceiling.

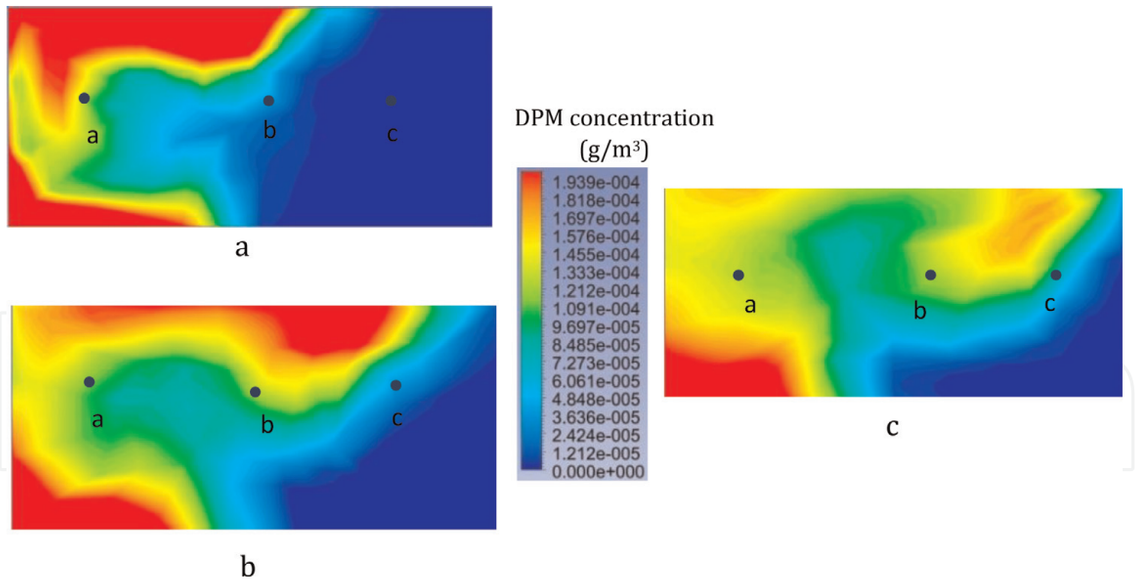

Figure 9.
DPM concentration at 1, 5 and 10 m downstream of the vehicle. (a) DPM concentration 1 m downstream of the vehicle. (b) DPM concentration at 5 m downstream of the vehicle. (c) DPM concentration 10 m downstream of the vehicle.

Sampling point	At sample station 1 m			At sample station 5 m		
	Experimental value (μg/m^3)	Simulation value (μg/m^3)	Difference %	Experimental value (μg/m^3)	Simulation value (μg/m^3)	Difference %
a	185.8	176	−5.2	149.0	130	−12.7
b	50	46	−8.0	117	110	−5.9
c	0	0	0	16	16	0
	At sample station 10 m					
a	127.4	130	2.0			
b	116.6	100	−14.2			
c	50.0	57	14.0			

Table 3.
Comparison of simulated results with experimental results.

from the measured data. This may be because the uneven texture of the gallery surface was not considered in the CFD model.

4.3 Experiment-1 DPM model validation

Table 3 shows the compared results of base case simulations and field experiments at 1, 5 and 10 m downstream of the vehicle and at the sample point a, b and c. The simulated results were in fair agreement with the measured data at a number of instances and such results which slightly deviated from the measured data can be due uneven gallery walls surface were not considered while modeling. The difference varies from −14.2 to +14%.

4.4 DPM exposure levels for passenger during vehicle movement

DPM concentration was measured in the passenger seat during vehicle movement. The vehicle engine was assumed to run at full capacity so that the engine

emitted maximum amount of fumes. DPM measurements were recorded as the vehicle traveled from the pit bottom to the work place, a distance of 4 km. The maximum speed of the vehicle on level ground is 25 km/h. During the experiment, the average velocity of the vehicle was 10 km/h (2.7 m/s). **Figure 10** shows the DPM concentration at different time periods during 4 km travel distance. The concentration changes with relative velocities between vehicle and air.

4.5 Changes of DPM concentration with intake air velocity

To understand the effect of intake air velocity on DPM dispersion, simulation studies were conducted with the air velocity ranging from 0.5 to 3 m/s.

Figure 11 shows the DPM concentration in the vertical mid-plane of the mine gallery when the intake air velocity is 0.5 m/s. The results show that high DPM concentration of over 200 μg/m^3 is observed in almost the entire roadway. High DPM concentration is also observed on the passenger side of the vehicle. Downstream of the vehicle, high DPM concentration spreads across almost the entire cross-section of the roadway.

Figure 12 shows the DPM concentration corresponding to an intake air velocity 3 m/s. most of the DPM concentration is at the smoke pipe side of the gallery roof

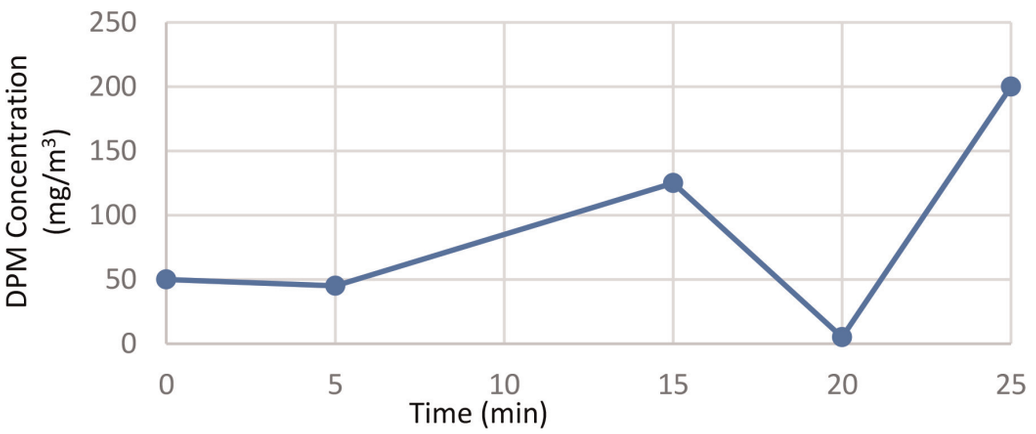

Figure 10.
EC concentration at passenger seat (moving vehicle).

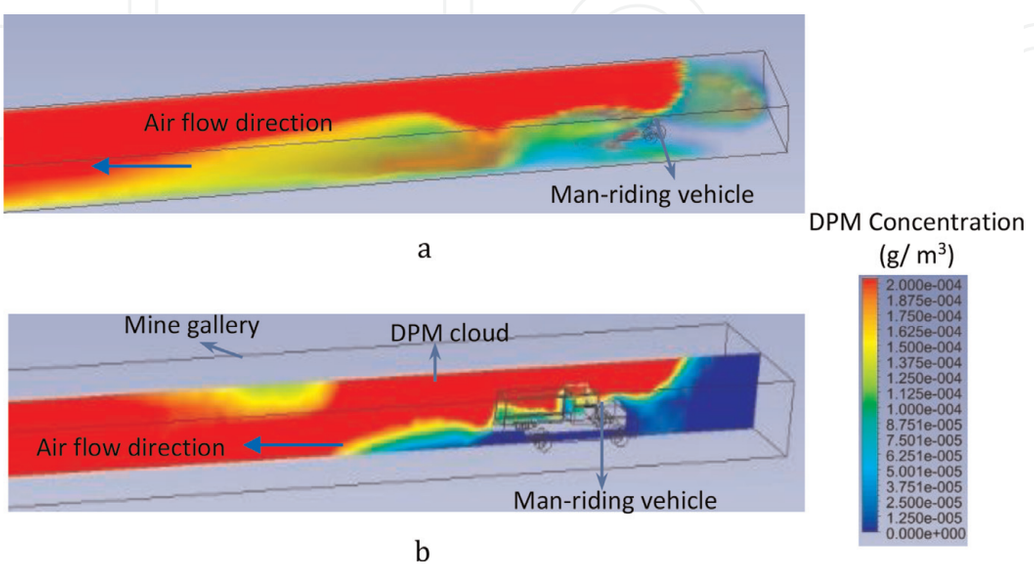

Figure 11.
DPM distribution with 0.5 m/s air velocity, center section of the mine gallery. (a) DPM concentration at mine gallery. (b) DPM concentration in vertical mid-plane of the gallery.

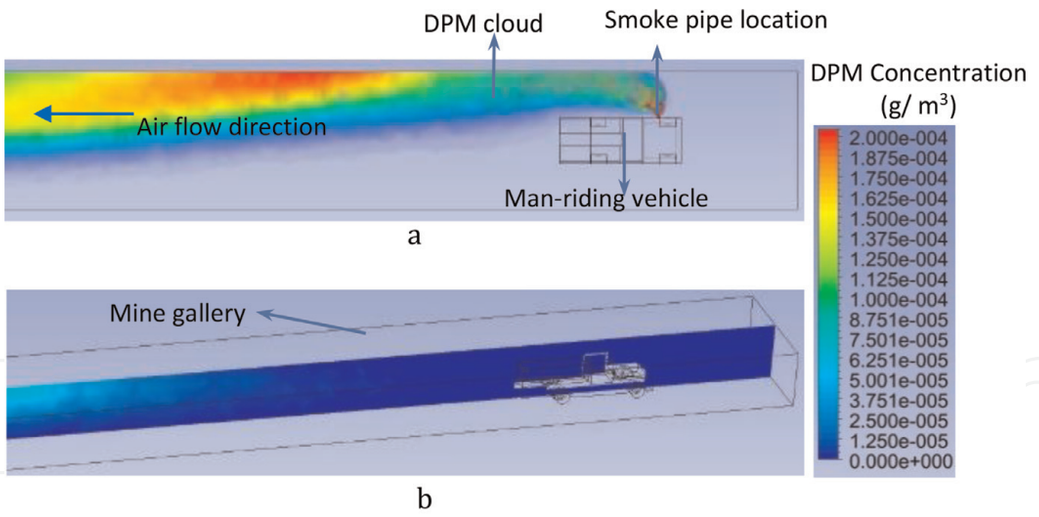

Figure 12.
DPM distribution with 3 m/s air velocity, top and center section view of mine gallery. (a) DPM concentration at mine gallery, top view. (b) DPM concentration in vertical mid-plane of the gallery.

due to high air velocity. Negligible DPM concentration was observed at the middle of the roadway up to 20 m downstream of the vehicle. Beyond 20 m downstream of the vehicle, DPM concentration of 60 μg/m^3 is observed near the ceiling and concentration reduced to zero towards the floor.

5. Results and discussions—experiment 2

5.1 DPM and air flow in opposite directions

Figure 13 shows the results of CFD simulations in isometric view when DPM and air flow are in opposite directions (counter-flow). Near the LHD, it can be observed that high DPM concentration is at middle of the gallery and above the LHD. At downstream side of the LHD, DPM particles spreads throughout the gallery, with the maximum concentration is in the middle and at sides of the gallery.

Figure 14 shows the DPM concentration patterns at 2, 5 and 8 m downstream of the vehicle rear end. **Figure 14(a)** shows the high DPM concentration near the top and bottom portions of the vehicle. **Figure 14(b)** shows the maximum

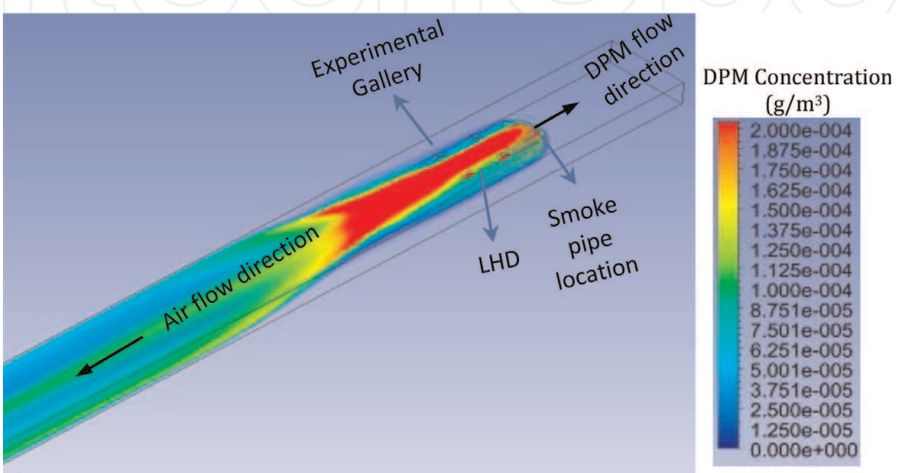

Figure 13.
DPM flow pattern—isometric view.

concentration is at top and bottom portions of the vehicle, concentrations also spreads at left and right sides of the road ways. DPM concentration at LHD operator is 125 μg/m^3. **Figure 14(c)** shows the DPM flow moved towards the roof and bottom of the road way, DPM concentration spreads at towards left and right sides of the road way.

Figure 15 shows the DPM concentration field at 6, 10 and 20 m downstream of the vehicle. **Figure 15(a)** shows the DPM concentration at 6 m downstream of the vehicle. Here, high DPM concentration is observed near the floor of the roadway, and the concentrations gradually reduces towards the roof.

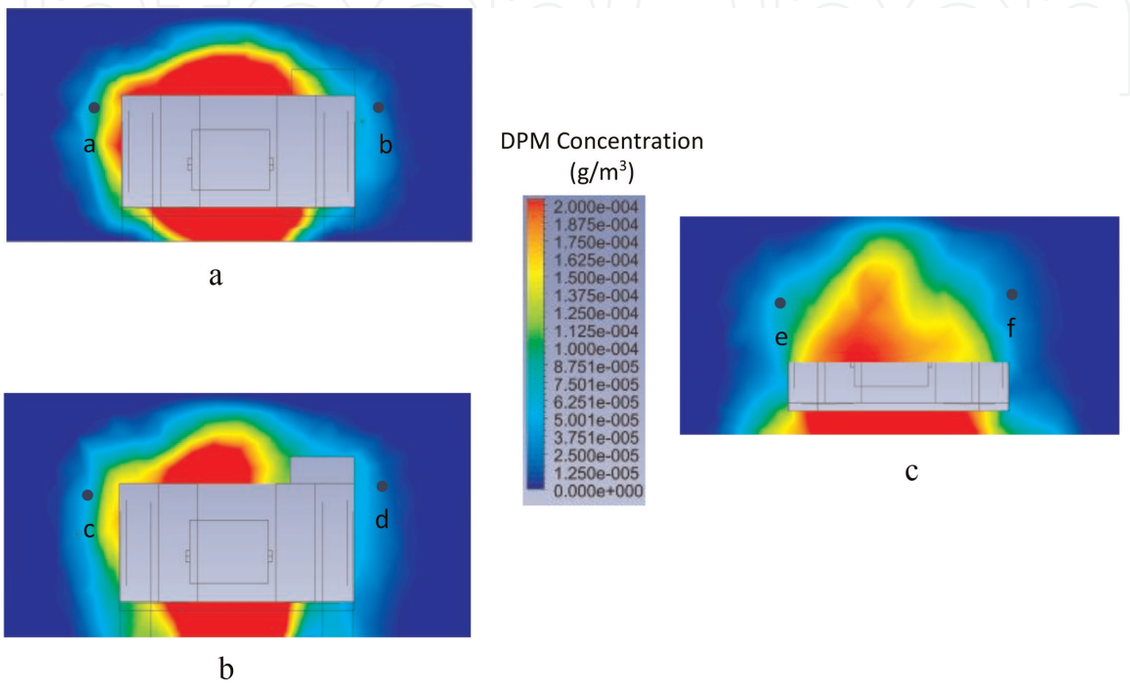

Figure 14.
DPM concentration at 2, 5 and 10 m downstream of the vehicle. (a) DPM concentration at 2 m downstream of the smoke pipe. (b) DPM concentration at 5 m downstream of the smoke pipe. (c) DPM concentration at 8 m downstream of the smoke pipe.

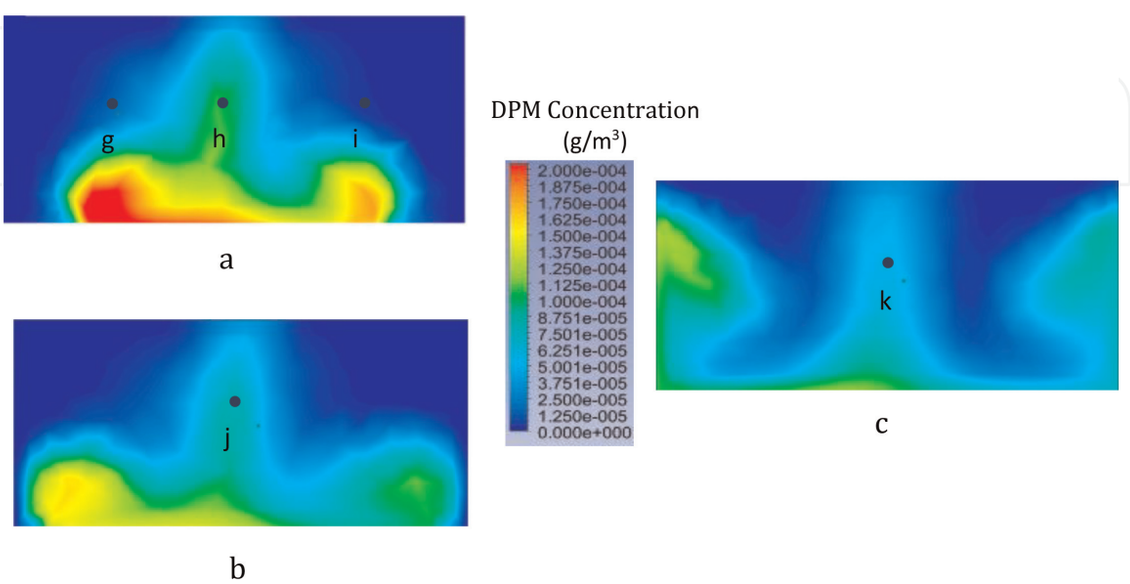

Figure 15.
DPM concentration at 2, 5 and 10 m downstream of the vehicle. (a) DPM concentration at 6 m downstream of the vehicle. (b) DPM concentration at 10 m downstream of the vehicle. (c) DPM concentration at 20 m downstream of the vehicle.

Figure 15(b) shows the DPM concentration field at 10 m downstream of the vehicle. Here, the maximum concentration is at middle of the gallery and left and right sides of the road ways.

Figure 15(c) shows the DPM concentration field at 20 m downstream of the vehicle. Here, the DPM is found to spread throughout the entire roadway. The DPM concentration at the center of the road way is 34 μg/m^3 and similar concentrations observed at left and right sides of the road way.

5.2 Experiment-2 DPM model validation

Table 4 compares the experimental results (ER) and simulation results of spot values of DPM concentration results at downstream side of the vehicle at different sampling points. From the table it can be observed that the simulated results were in fair agreement with the measured data, the difference is varies from −21 to +21%.

5.3 DPM flow pattern when air flow and DPM in the same direction

Figure 16 shows the results of CFD simulations in isometric view when DPM and air flow are in the same direction (co-flow). High DPM concentration is observed in the middle of the gallery. At 50 m downstream of the vehicle, DPM particles are seen to spread over most of the middle gallery.

Sample point	ER	SR	Difference %	Sample point	ER	SR	Difference %
2 m to source (a)	—	125	—	6 m to vehicle (g)	14	17	21
2 m to source (b)	70	55	−21	6 m to vehicle (h)	42	48	14
5 m to source (c)	56	60	7	6 m to vehicle (i)	26	25	−3
5 m to source (d)	55	43	−21	10 m to vehicle (j)	42	48	14
8 m to source (e)	42	35	−16	20 m to vehicle (k)	28	34	21
8 m to source (f)	27	27	0				

Table 4.
Comparison of simulated results (SR in μg/m³) with experimental results (ER in μg/m³).

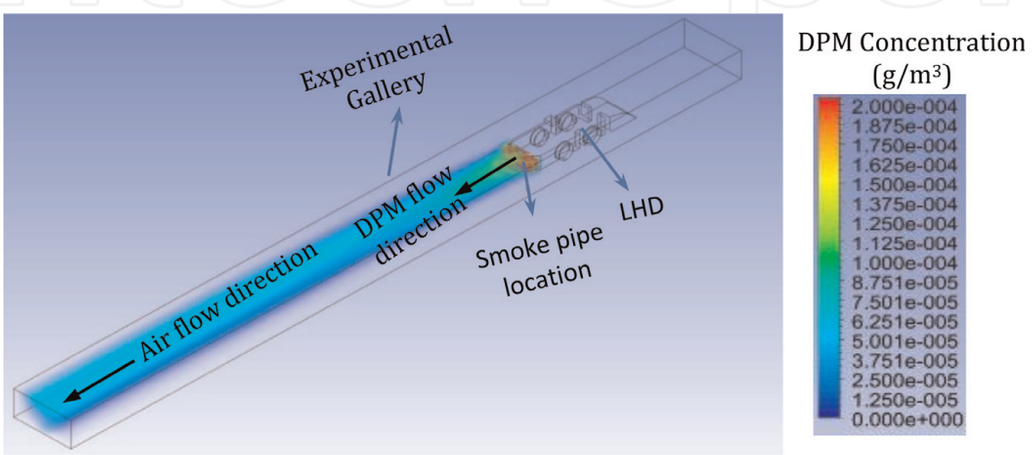

Figure 16.
DPM flow pattern for co-flow (flows in the same direction).

6. Conclusions

In this study, field measurements and CFD simulations were used to map contours of diesel particulate matter (DPM) generated by a man riding vehicle and an LHD located in the gallery of an underground mine. CFD models were validated against the field experimental data, and simulation results were found to be in fair agreement with the measured data. Studies with a man-riding vehicle showed that if the vehicle is stationary, high DPM concentration tends to flow moves towards the center of the gallery. At 20 m downstream of the vehicle, DPM particles spread throughout the entire roadway. Studies also shows that DPM concentration levels reduce with increase in ventilation air velocity. Experiments showed that during vehicle movement, the passenger may be exposed to higher DPM concentration due to airflows induced by the vehicle movement.

The LHD studies show that if the DPM flow and ventilation air co-flow (are in the same direction), the DPM is confined predominantly to the middle of the road way. If the DPM flow and the ventilation air flow are in counter-flow (opposite directions), the DPM spreads throughout the entire cross-section of the roadway. In this case, the vehicle operator will be more susceptible to exposure to high concentrations of DPM.

Acknowledgements

The authors sincerely thank M/s Coal India Limited, DGMS, Govt. of India and IIT (ISM) Dhanbad for providing the necessary resources and extending cooperation during the field experiments.

Conflict of interest

On behalf of all authors, the corresponding author affirms that there is no conflict of interest.

Nomenclature

ACGIH	American Conference of Governmental Industrial Hygienists
CANMET	Canada Centre for Mineral and Energy Technology
CFD	computational fluid dynamics
CO	carbon monoxide
DEEP	diesel emissions evolution program
DPF	diesel particulate filter
DPM	diesel particulate matter
EC	elemental carbon
ER	experimental results
HC	hydrocarbons
LHD	load haul dumper
MSHA	Mine Safety and Health Administration
NIOSH	National Institute of Occupational Health and Safety
NMA	National Mining Association
NMHC	non-methane hydrocarbons
NOx	nitrogen oxides

NSSGA	National Stone, Sand and Gravel Association
OC	organic carbon
OEL	occupational exposure limits
RCD	respirable combustible dust
STEL	short term exposure limit
TC	total carbon
TWA	time weighted average
USWA	United Steel Workers of America
WHS	Work Health and Safety

Author details

Ramakrishna Morla[1*], Shivakumar Karekal[2] and Ajit Godbole[2]

1 CSA Mine, Glencore, Cobar, NSW, Australia

2 School of Civil, Mining and Environmental Engineering, University of Wollongong, Australia

*Address all correspondence to: ramsiit99@gmail.com

References

[1] AIOH. Diesel Particulate Matter & Occupational Health Issues. Position Paper. AIOH Exposure Standards Committee. 2013. Available from: https://www.aioh.org.au/documents/item/15 [Accessed: 09 December 2018]

[2] Bugarski AD, Janisko SJ, Cauda EG, Noll JD, Mischler SE. Controlling Exposure to Diesel Emissions in Underground Mines. Englewood, Colorado: Society for Mining, Metallurgy, and Exploration, Inc. (SME); 2012

[3] MDG 29 (Mine Design Guideline 29). Guideline for the Management of Diesel Engine Pollutants in Underground Environments. Produced by Mine Safety Operations Division, New South Wales Department of Primary Industries. 2008. Available from: http://www.resourcesandenergy.nsw.gov.au/__data/assets/pdf_file/0011/419465/MDG-29.pdf

[4] Work Health and Safety (Mines and Petroleum Sites) Regulations. 2014. Available from: https://www.legislation.nsw.gov.au/inforce/500011c6-2a99-440f-8799-8cbf39393930/2014-799.pdf [Accessed: 17 December 2018]

[5] Work Health and Safety (Mines and Petroleum Sites) Act. 2013. Available from: https://www.legislation.nsw.gov.au/inforce/2452de08-45ac-4954-856f-af17f88c9fc3/2013-54.pdf [Accessed: 09 December 2018]

[6] Coal Mines Health and Safety Regulations. 2006. Australia. Available from: http://www.dpi.nsw.gov.au/__data/assets/pdf_file/0018/101745/CMHS-Regulation-2006.pdf [Accessed: 17 December 2018]

[7] David BK. Measurement of Engine Exhausts Particle Size. University of California; 2002. Available from: http://www.me.umn.edu/centers/mel/reports/dbkucdavis.pdf

[8] Attfield MD, Schleiff PL, Lubin JH, Blair A, Stewart PA, Vermeulen R, et al. The diesel exhaust in miners study: A cohort mortality study with emphasis on lung cancer. Journal of the National Cancer Institute. 2012;**104**(11):869-883. DOI: 10.1093/jnci/djs035

[9] Silverman D, Samanic C, Lubin J, Blair E, Stewart P, Vermeulen R, et al. The Diesel Exhaust in Miners Study: A Cohort Mortality Study with Emphasis on Lung Cancer. Oxford University Press; 2011. Available from: https://www.ncbi.nlm.nih.gov/pmc/articles/PMC3369553/pdf/djs034.pdf

[10] Cox A, Costle D, King S, Huang A, Stewart R, Kennedy D, et al. Diesel Emissions and Lung Cancer. Epidemiology and Quantitative Risk Assessment. Health Effect Institute; 1999. Available from: https://www.healtheffects.org/system/files/DieselEpi.pdf [Accessed: 09 December 2018]

[11] Bartlett CJS, Betts WE, Booth M, Giavazzi F, Guttmann H, Heinze P, et al. The Chemical Composition of Diesel Particulate Emissions. Report No. 92/51. 1992. Available from: https://www.concawe.eu/wp-content/uploads/2017/01/rpt_92-51ocr-2004-01337-01-e.pdf

[12] Gangal M. Summary of Worldwide Underground Diesel Regulations, CANMET Mining. 2012. Available from: http://www.mdec.ca/2012/S3P3-Gangal.pdf [Accessed: 15 January 2019]

[13] Bugarski A, George S, Jim N, Steve M, Larry P, Jon H, et al. The Effectiveness of Selected Technologies in Controlling Diesel Emissions in an Underground Mine Isolated Zone Study at Stillwater Mining company's Nye

Mine. Final Report to Metal/Non-Metal Diesel Partnership. 2004. Available from: https://stacks.cdc.gov/view/cdc/9387/cdc_9387_DS1.pdf? [Accessed: 15 January 2019]

[14] McGinn S, Grenier M, Gangal M, Rubeli B, Bugarski A, Schnakenberg G, et al. Final Report of Investigation to the Diesel Emissions Evaluation Program (DEEP), Noranda Inc.-Brunswick Mine Diesel Particulate Filter (DPF) Field Study. 2004. Available from: https://www.cdc.gov/niosh/mining/UserFiles/works/nordpf_final.pdf [Accessed: 15 January 2019]

[15] Zheng Y. Diesel particulate matter dispersion analysis in underground metal/non-metal mines using CFD [thesis]. Missouri University of Science and Technology; 2011, 2011. Available from: https://scholarsmine.mst.edu/cgi/viewcontent.cgi?article=3018&context=doctoral_dissertations

[16] Janisko S, Noll J. Near real time monitoring of diesel particulate matter in underground mines. In: 12th U.S/North American Mine Ventilation Symposium; 9-11 June 2008; Reno, NV. 2008. pp. 509-513

[17] Khan UM. Real-time diesel particulate matter monitoring in underground mine atmospheres, association with the standard method and related challenges [thesis]. Missouri University of Science and Technology; 2017. Available from: http://scholarsmine.mst.edu/doctoral_dissertations/2625/

[18] Flir Airtec DPM Monitor. Available from: https://www.flir.com/globalassets/imported-assets/.../airtec-datasheet-english.pdf [Accessed: 15 January 2019]

[19] Zheng Y, Magesh T, Lan H, Ten CJ. Simulation of DPM distribution in a long single entry with buoyancy effect. International Journal of Mining Science and Technology. 2016;**25**(1):47-52. DOI: 10.1016/j.ijmst.2014.11.004

[20] Zheng Y, Magesh T, Lan H, Ten CJ. Effect of auxiliary ventilations on diesel particulate matter dispersion inside a dead-end entry. International Journal of Mining Science and Technology. 2015; **25**(6):927-932. DOI: 10.1016/j.ijmst.2015.09.008

[21] Zheng Y, Magesh T, Lan H, Tien CJ. Simulation of DPM distribution in a long single entry with buoyancy effect. International Journal of Mining Science and Technology. 2015;**25**(1):47-52

[22] Zheng Y, Lan H, Magesh T, Tien JC. DPM dispersion experiment at MST's experimental mine and comparison with CFD simulation. Journal of Coal Science and Engineering. 2011;**17**(3):285-289. DOI: 10.1007/s12404-011-0311-1

[23] Morla R, Godbole A, Karekal S, Bhattacharjee R, Nasina B. Fundamental understanding of diesel-operated man riding vehicle DPM dispersion—A case study. Journal of Sustainable Mining. 2018;**17**(3):105-110

[24] Morla R, Karekal S. Diesel particulate matter investigations in underground coal mines. International Journal of Engineering and Technology. 2018;**9**(4):2698-2703. Available from: http://www.enggjournals.com/ijet/abstract.html?file=17-09-04-401

[25] ANSYS Fluent Theory Guide. Canonsburg, PA: ANSYS, Inc; 2013